

Supplementary Information

S-doped TiN Supported N, P, S-tridoped TiO₂ with Hetero-phase Junctions for Fuel Cell Startup/Shutdown Durability

Mitsuharu Chisaka, Jubair A. Shamim, Wei-Lun Hsu and Hirofumi Daiguji*

M. Chisaka

Department of Sustainable Energy, Hirosaki University, 3 Bunkyo-cho, Hirosaki, Aomori 036-8561, Japan. E-mail: chisaka@hirosaki-u.ac.jp.

J. A. Shamim, W.-L. Hsu and H. Daiguji

Department of Mechanical Engineering, The University of Tokyo, 7-3-1, Hongo, Bunkyo-ku, Tokyo 113-8656, Japan.

S1. Experimental details

Catalyst synthesis: N, P-TiO₂/S-TiN catalysts were synthesized using a recently reported solution phase combustion route^{S1} then they were converted to N, P, S-TiO₂/S-TiN catalysts by an annealing step developed in this study. First, 0.49 g of titanium oxysulfate powder (TiOSO₄·*n*H₂O; *n* ≐ 1~2, Kishida Chemical Co. Ltd., Osaka, Osaka, Japan) was dispersed in 371 cm³ of distilled water by stirring at room temperature in a polytetrafluoroethylene (PTFE) beaker whose outside bottom was coated with a PTFE-carbon composite to facilitate heating on a hot stirrer. Second, 97 mm³ of 30% w/w H₃PO₂ solution (Fuji Film Wako Pure Chemical Co., Osaka, Osaka, Japan) was added with continuous stirring to set the optimum atomic ratio of phosphorous to titanium, 0.20.^{S1} Third, 20 g of urea powder ((NH₂)₂CO, Fuji Film Wako Pure Chemical Co., Osaka, Osaka, Japan) was added to set the mass ratio of urea to TiOSO₄-derived TiO₂ at 100. Fourth, 36 cm³ of 35% w/w HCl solution (Kishida Chemical Co. Ltd., Osaka, Osaka, Japan) was added to the solution with continuous stirring. Then, the PTFE beaker was placed on another stirrer preheated to 523 K and stirred continuously until the water evaporated. Fifth, the beaker was then placed onto a hot plate that was preheated to 473 K and kept overnight. The mixing and drying procedures, i.e., all of the first to fifth steps were performed in a fume hood. After the drying, the obtained powders were ground using an agate mortar and placed in an alumina boat. The boat was set in a horizontal quartz-tube furnace that was placed in the fume hood. The tube was slowly evacuated and purged with N₂ gas. The powder samples were heated from room temperature to 1,173 K at a rate of 10 K min⁻¹ and maintained for 2 h. The 1,173 K of pyrolysis temperature is 50 K higher than the previously optimized 1,123 K,^{S1} as a larger furnace with a larger tube was used in this study to increase the batch size. The samples were then cooled to room temperature at an uncontrolled rate. The N₂ flow rate was 0.1 dm³ min⁻¹ during pyrolysis. After pyrolysis, the powders were ground in an agate mortar to obtain N, P-TiO₂/S-TiN. Some solid by-products

attached to the inner wall of the quartz tube during pyrolysis, which can stop the gas flow if they block the narrow opening of the quartz tube. Therefore, a quartz tube more than three times longer than the heating zone was used to provide sufficient space for by-product accumulation inside the tube to avoid blockage by solid by-products. The by-products were removed by washing the tube with water and heating without any sample in air at 1,300 K for ca. 2 h. The obtained N, P-TiO₂/S-TiN catalysts and ammonia fluoride (NH₄F, Fuji Film Wako Pure Chemical Co., Osaka, Osaka, Japan) were ground in an agate mortar then the mixture was placed in an alumina boat and then the boat was placed in another horizontal quartz tube furnace, purged with flowing N₂ gas for at least 600 s. Then the mixture samples were heated from room temperature to various temperatures at a rate of ca. 20 K min⁻¹. The duration, N₂ flow rate and the mass ratio of NH₄F to N, P-TiO₂/S-TiN were set at 1 h, 0.5 dm³ min⁻¹ and 3, respectively unless otherwise noted. Finally, the samples were cooled without controlling the cooling rate to obtain N, P, S-TiO₂/S-TiN. After the annealing, the tube was washed with water then heated without any sample in air at 1,300 K for ca. 2 h to remove any byproducts. All the steps for synthesizing N, P, S-TiO₂/S-TiN from N, P-TiO₂/S-TiN were performed in the fume hood. For reference, TiOSO₄·nH₂O was replaced with a sulfur-free titanium source, diammonium hexafluorotitanate ((NH₄)₂TiF₆, Fuji Film Wako Pure Chemical Co., Osaka, Osaka, Japan) then N, P-TiO₂/TiN catalysts were synthesized under conditions identical to those of N, P, S-TiO₂/S-TiN catalysts which exhibited the highest oxygen reduction reaction (ORR) activity.

Characterization: The bulk crystal structures of N, P-TiO₂/S-TiN and N, P, S-TiO₂/S-TiN catalysts were evaluated using an X-ray diffractometer (MiniFlex 600, Rigaku Co., Akishima, Tokyo, Japan) with Cu-K α radiation generated at 40 kV and 15 mA (scan range = 20–80°, step size = 0.02°, and scan rate = 2° min⁻¹). The crystal structure of the outermost surface of N, P, S-TiO₂/S-TiN was evaluated using a Raman spectrometer (LabRAM HR-evolution, Horiba Scientific Co. Ltd., Kyoto, Kyoto,

Japan) equipped with a 325 nm laser. The morphology of the catalysts was investigated using a transmission electron microscope (JEM-2100, JEOL Inc., Akishima, Tokyo, Japan). The chemical states of the catalysts were determined using an X-ray photoelectron (XP) spectrometer (PHI VersaProbeIII, ULVAC-PHI, Inc., Chigasaki, Kanagawa, Japan) with an Al-K α X-ray source (1486.6 eV). The peak shifts due to surface charge were corrected using the binding energy of the C 1s (284.8 eV) of the organic contaminants from the spectrometer and/or air. The Ti 2p, N 1s and S 2p spectra were analyzed by fitting six, four and four symmetric peaks, respectively, after subtracting a Shirley-type background. The bulk composition of the catalysts was determined using an energy dispersive (ED) X-ray spectrometer (JED-2300F, JEOL Inc., Akishima, Tokyo, Japan).

ORR activity and selectivity measurements: Rotating disk electrode (RDE) and rotating ring-disk electrode (RRDE) voltammograms were obtained to evaluate the ORR activity and selectivity, respectively, of the catalysts. The catalyst, 5% w/w Nafion® ionomer solution (510211, Sigma-Aldrich Co., St. Louis, Missouri, U.S.), and isopropyl alcohol were sonicated for 1200 s and then further mixed using a planetary mixer (Mazuru Star KK-250S, Kurabo Co., Osaka, Osaka, Japan) for 180 s to obtain a homogeneous catalyst ink. The mass fraction of Nafion in the catalyst layer was set at 0.05. The catalyst loading, m , was constant at 0.86 mg cm⁻², unless otherwise noted, by dropping 6.4 mm³ of the catalyst ink onto a glassy carbon (GC) disk (4 mm diameter)–platinum ring (5 mm inner diameter and 7 mm outer diameter) electrode (012613, BAS Co., Sumida-ku, Tokyo, Japan). Prior to the treatment, the surface of the GC disk electrode was polished with 1.0- and 0.05- μ m alumina slurries, cleaned with distilled water and ethanol, and then air-dried at 320 K for at least 600 s. A conventional three-electrode cell was used for the room-temperature electrochemical measurements performed in 0.1 mol dm⁻³ H₂SO₄ solution. The catalyst-coated GC disk–Pt ring electrode, a carbon rod (diameter: 5 mm, C-072591, Nilaco Co., Chuo-ku, Tokyo, Japan), and a Ag/AgCl

(sat. KCl) electrode (HS-205C, TOA DKK Co., Shinjuku-ku, Tokyo, Japan) were used as the working, counter, and reference electrodes, respectively. The working electrode was placed on a rotator (RRDE-3A, BAS Co., Sumida-ku, Tokyo, Japan). All the working electrode potentials were referenced to the reversible hydrogen electrode (RHE). After sequentially bubbling O₂ and N₂ for 1800 s, the RDE and RRDE voltammograms were recorded by applying a disk potential, E_d , from 1.2 to 0.1 V at a cathodic scan rate of 5 mV s⁻¹ and a rotation speed of 1500 rpm using a bipotentiostat (Model 2323, 700B or 704B, BAS Co., Sumida-ku, Tokyo, Japan). The ring potential was maintained at 1.2 V to obtain the RRDE voltammograms. The ORR current density was measured after the background correction by $j = j_O - j_N$, the difference between the current per unit geometrical area of the GC disk electrode obtained in O₂- (j_O) and in N₂-saturated electrolyte (j_N). The hydrogen peroxide yield, $X_{\text{H}_2\text{O}_2}$, and number of electrons transferred per unit oxygen molecule, n , were calculated by analyzing the RRDE voltammograms according to equation (S1) and equation (S2), respectively:

$$X_{\text{H}_2\text{O}_2} (\%) = 100 \cdot \frac{2I_r / N}{-I_d + I_r / N} \quad (\text{S1})$$

$$n = \frac{-4I_d}{-I_d + I_r / N} \quad (\text{S2})$$

where I_d and I_r denote the disk and ring currents, respectively, after the background correction described above, and N is the collection efficiency (0.424) provided by the manufacturer (BAS Co.). Nyquist plots were measured by applying a root mean square alternating current voltage at 5 mV in the frequency range from 1 to 1.0 MHz at 0.7 V versus the RHE in an O₂-saturated 0.1 mol dm⁻³ H₂SO₄ solution using a potentiostat equipped with a frequency response analyzer (SP-150, Bio-Logic Science Instruments, Seyssinet-Pariset, Isère, France), which was connected to the three-electrode cell used for the abovementioned ORR activity and selectivity measurements. The solution resistance between the working electrode and

reference electrode, R , was determined by the high-frequency intercept of the Nyquist plots, and all the E_d values were corrected with the resistance according to equation (S3).

$$E = E_d + |I_d|R \quad (\text{S3})$$

After the initial activity evaluation at $m = 1.50 \text{ mg cm}^{-2}$, accelerated degradation tests were performed using a startup/shutdown protocol for automotive fuel cells proposed by the fuel cell commercialization conference in Japan (FCCJ),^{S2} in which E_d was cycled between 1.0 and 1.5 V at a scan rate of 0.5 V s^{-1} in N_2 -saturated electrolyte. After 5,000 cycles, the ORR activity was evaluated as described above. The amount of titanium ions dissolved in the electrolyte solution after 5,000 startup/shutdown cycles were measured using an inductively coupled plasma (ICP) spectrometer (5100 ICP-OES, Agilent Technologies. Inc., Santa Clara, California, U.S.).

S2. Crystal structures and chemical states of N-TiO₂/S-TiN and N, P-TiO₂/S-TiN catalysts

Fig. S1 shows XRD patterns and Raman spectra of previously reported N-TiO₂/S-TiN^{S3} and N, P-TiO₂/S-TiN catalysts synthesized by using two different phosphorous sources, H₃PO₂^{S1} and H₃PO₄.^{S3} All the N-TiO₂/S-TiN and N, P-TiO₂/S-TiN catalysts display a single TiN phase. The single TiN phase of the N, P-TiO₂/S-TiN catalyst is well reproduced in this study as shown in Fig. 1(b) despite the difference in the used quartz tube, tube furnace and N₂-pyrolysis temperature as described in section **S1**. The Raman spectra were acquired with a 532 nm-laser. All catalysts display two peaks at ~410 cm⁻¹ and ~600 cm⁻¹, which are assigned to the optical vibration modes, E_g and A_{1g}, respectively of rutile TiO₂ with oxygen vacancies.^{S1,S3}

Fig. S2 shows the XP spectra of N, P-TiO₂/S-TiN catalysts. The peak binding energies of previously reported N, P-TiO₂/S-TiN catalysts in Ti 2p, N 1s and P 2p regions shown in Fig. S2 are same as those of N, P, S-TiO₂/S-TiN catalyst shown in Fig. 1(e). The area fraction of N-doped TiO₂ phase in the Ti 2p region of N, P, S-TiO₂/S-TiN catalyst shown in Fig. 1(e) is substantially lower than that of N, P-TiO₂/S-TiN catalysts shown in Fig. S2 because N, P, S-TiO₂/S-TiN catalyst was oxidized by NH₄F-annealing as revealed by XRD analyses with Fig. 1(b).

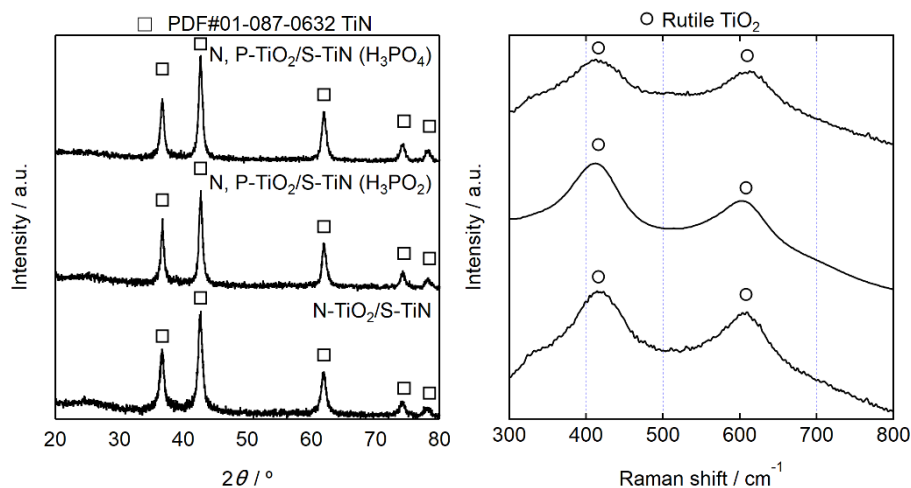


Fig. S1 (Left) X-ray diffraction (XRD) patterns and (right) Raman spectra of N-TiO₂/S-TiN (bottom) and N, P-TiO₂/S-TiN catalysts synthesized using two different phosphorous sources, H₃PO₂ (middle)^{S1} and H₃PO₄ (top).^{S3} Reproduced with permissions.^{S1,S3}

Copyrights 2019, 2020, Royal Society of Chemistry, American Chemical Society.

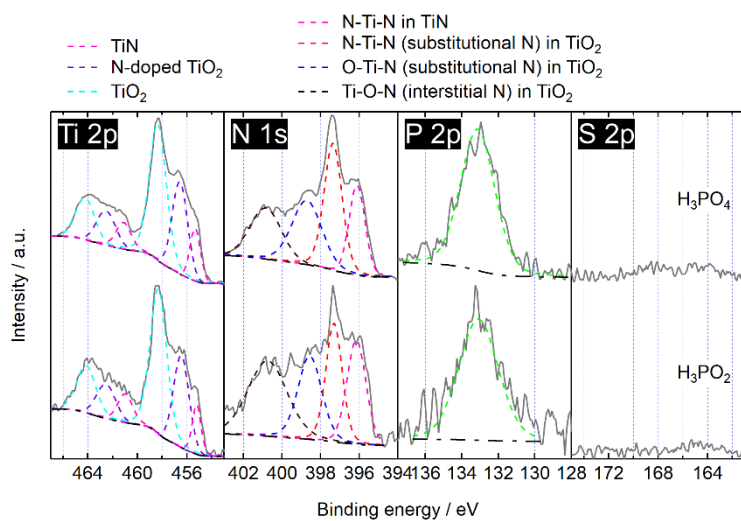


Fig. S2 X-ray photoelectron (XP) spectra of N, P-TiO₂/S-TiN catalysts synthesized using two different phosphorous sources, H₃PO₂^{S1} and H₃PO₄.^{S3} Reproduced with permissions.^{S1,S3} Copyrights 2019, 2020, Royal Society of Chemistry, American Chemical Society.

S3. Effect of NH₄F-annealing atmosphere on the crystal structure and ORR activity of N, P, S-TiO₂/S-TiN catalysts

Fig. S3 shows X-ray diffraction (XRD) patterns and RDE voltammograms of the N, P, S-TiO₂/S-TiN catalysts synthesized by annealing N, P-TiO₂/S-TiN with NH₄F at 1,223 K under three different flowing gases, N₂ with 0.5 dm³ min⁻¹, 10% v/v H₂/Ar with 0.1 dm³ min⁻¹ and 10% v/v H₂/Ar with 0.5 dm³ min⁻¹. A single TiN phase of N, P-TiO₂/S-TiN before annealing shown in Fig. 1(b) is oxidized to form the mixture of TiN and anatase/rutile TiO₂ phases after NH₄F-annealing under N₂. The mixed phases retains with substantially lower TiN content when the flowing gas is switched to 10% v/v H₂/Ar with 0.1 dm³ min⁻¹. When the H₂/Ar-flow rate is increased to 0.5 dm³ min⁻¹, a single TiN phase of N, P-TiO₂/S-TiN remains during the annealing. These results indicate that oxygen contaminants in the quartz tube used for the annealing reacted with the catalyst sample to form TiO₂ phases. We have previously reported that oxygen contaminants in flowing 5% v/v H₂/Ar gas react with Hf₂ON₂ nanoparticles at 1,223 K to oxidize them to form a HfO₂ phase.^{S3} Highly reductive 10% v/v H₂/Ar gas with a high flow rate used in this study suppresses the oxidation of TiN. However, the ORR activity decreases significantly by changing the gas from N₂ to 10% v/v H₂/Ar with the identical flow rate of 0.5 dm³ min⁻¹, indicating that the formation of the anatase/rutile mixture is necessary for the ORR activity. When the 10% v/v H₂/Ar gas flow rate is 0.1 dm³ min⁻¹ to have the mixture of TiN and anatase/rutile TiO₂ phases, the ORR activity is still lower than that obtained at N₂ with 0.5 dm³ min⁻¹ due to the lower TiN content to have insufficient conductivity of the catalyst given by TiN.

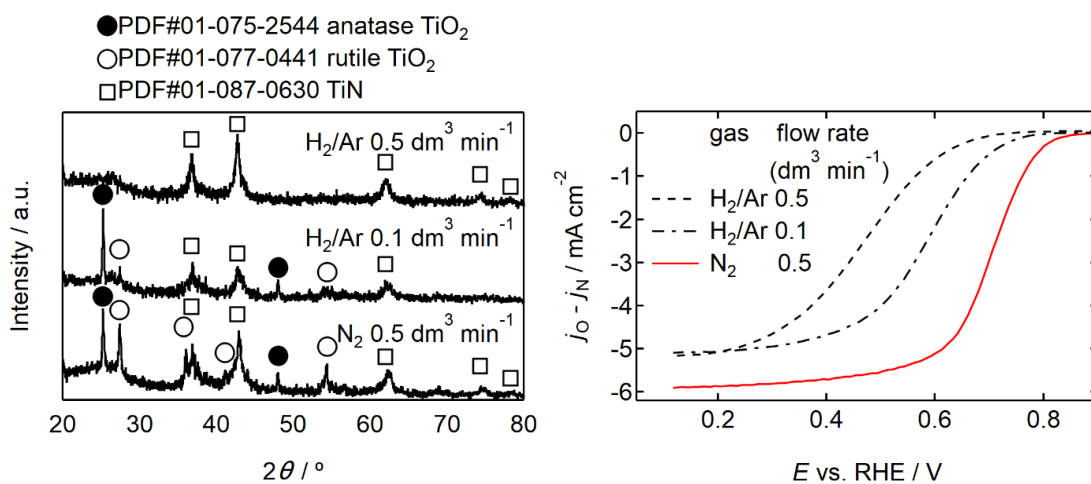
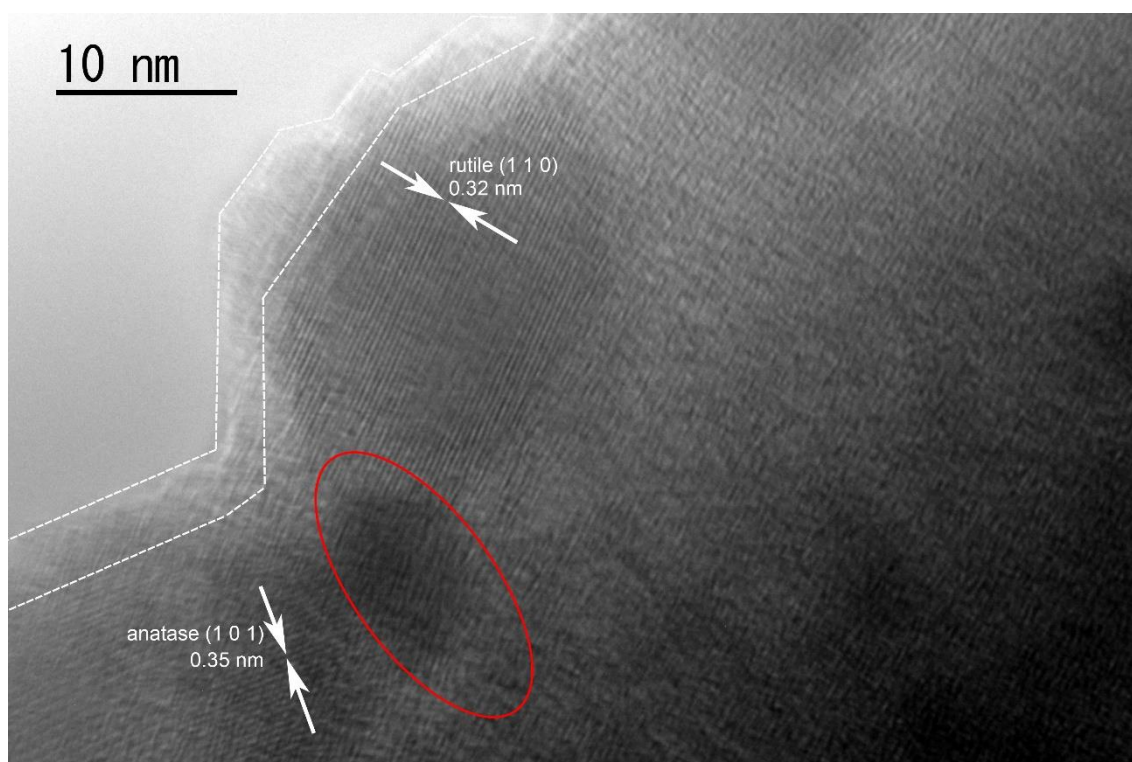
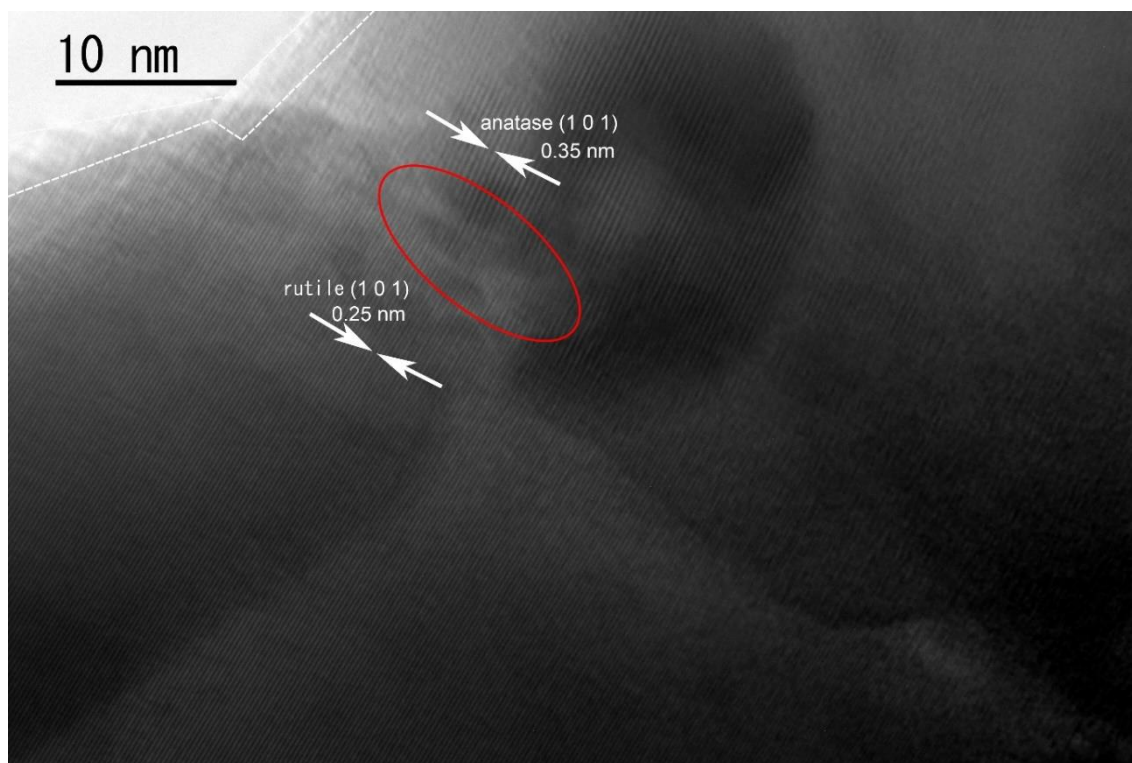


Fig. S3 (left) X-ray diffraction (XRD) patterns and (right) rotating disk electrode (RDE) voltammograms of N, P, S- TiO_2 /S-TiN after NH_4F -annealing at 1,223 K for 1 h under three different gas atmospheres, N_2 with 0.5 $\text{dm}^3 \text{min}^{-1}$, 10% v/v H_2/Ar with 0.1 $\text{dm}^3 \text{min}^{-1}$ and 10% v/v H_2/Ar with 0.5 $\text{dm}^3 \text{min}^{-1}$. The mass ratio of NH_4F to N, P- TiO_2 /S-TiN was fixed at 3 for all the catalysts. The scans were performed in N_2 and O_2 atmospheres at a rotation speed of 1,500 revolutions per minute (rpm) and a cathodic scan rate of -5 mV s^{-1} in 0.1 mol dm^{-3} H_2SO_4 solution.

S4. TEM images of N, P, S-TiO₂/S-TiN



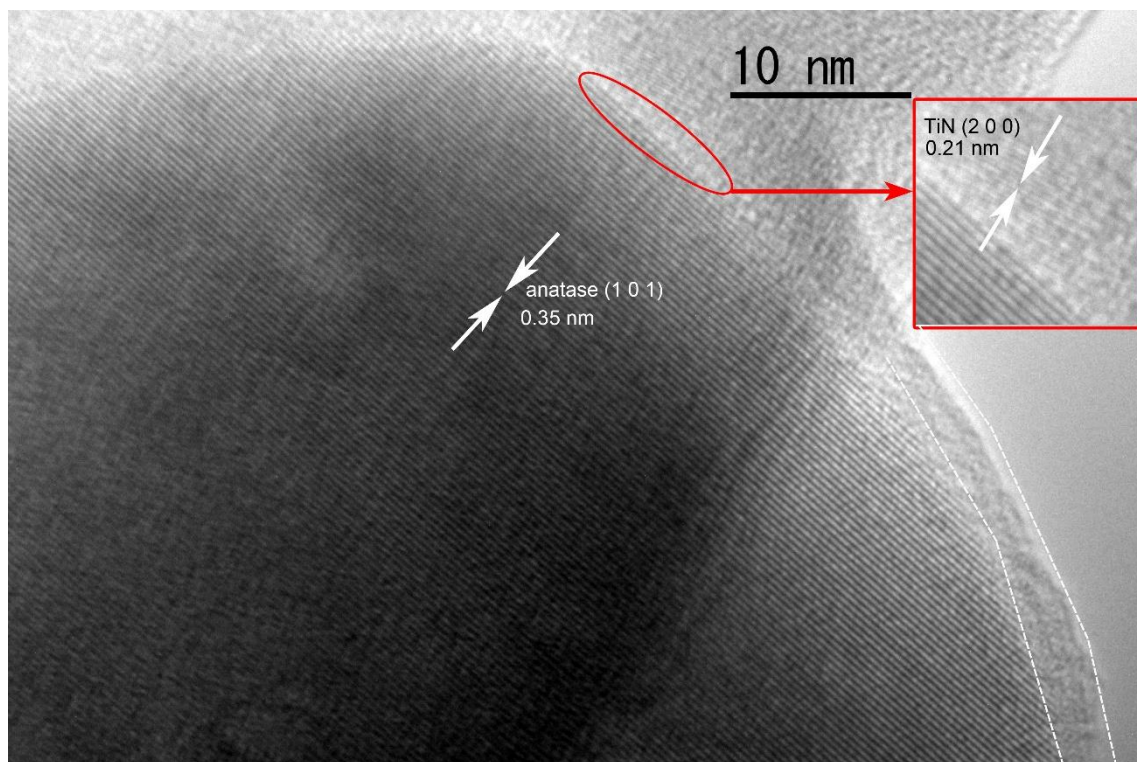


Fig. S4 Transmission electron microscopy (TEM) images of N, P, S-TiO₂/S-TiN.

S5. Surface analyses of elements from precursors

Fig. S5 shows a S 2p spectrum of N, P-TiO₂/S-TiN before NH₄F-annealing. No peaks are found from the spectrum, indicating the absence of sulfur species on the surface.

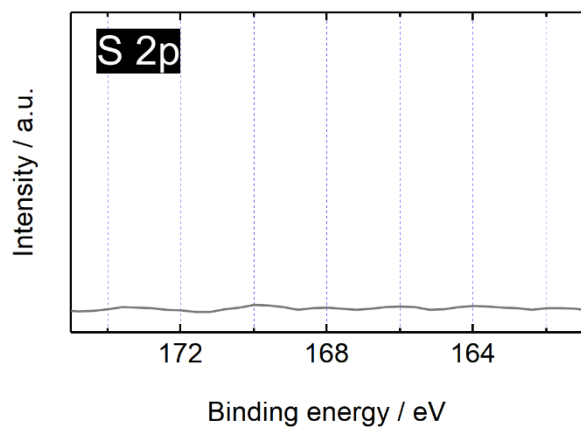


Fig. S5 A XP S 2p spectrum of N, P-TiO₂/S-TiN.

S6. Effect of the mass ratio of NH₄F to N, P-TiO₂/S-TiN on the crystal structure and ORR activity of N, P, S-TiO₂

Fig. S6 shows XRD patterns and RDE voltammograms of N, P, S-TiO₂/S-TiN catalysts synthesized by annealing the mixture of NH₄F and N, P-TiO₂/S-TiN at three different mass ratios of NH₄F to N, P-TiO₂/S-TiN, 1, 3 and 5. The TiN content decreases while anatase TiO₂ content increases when the NH₄F to N, P-TiO₂/S-TiN ratio is increased from 1 to 5, indicating that TiN is broken by NH₄F during the annealing at 1,223 K to form anatase/rutile TiO₂ phase. Anatase transforms irreversibly to rutile with increasing the temperature and the phase transition starts typically at 873–973 K in air for bulk pure TiO₂.^{S5} However, Yu *et al.* reported that fluorine ions released from NH₄F prevent the phase transition of anatase to rutile at 973 K in air.^{S6} Although the annealing temperature used to synthesize three N, P, S-TiO₂/S-TiN catalysts was much higher, 1,223 K and the annealing atmosphere was under N₂ gas flow, the results shown in Fig. S6 (left) indicate that NH₄F prevents the anatase to rutile transformation, similar to the previous work.^{S6} Besides, S²⁻ which substituted for O atoms in TiO₂ retained anatase phase as discussed in the main text. The NH₄F to N, P-TiO₂/S-TiN mass ratio significantly affects the ORR activity, as shown in Fig. S6 (right). The activity increases significantly with increasing the NH₄F to N, P-TiO₂/S-TiN mass ratio from 1 to 3 then decreases a little with a further increase to 5. These results indicate that active sites are produced with the formation of anatase/rutile TiO₂ mixture from TiN. The TiN is a well-known metallic nitride to display 4.6×10^4 S cm⁻¹ of electrical conductivity, which is 17 orders of magnitude higher than that of a semiconductor TiO₂.^{S7} Thus, ORR activity decreases when the NH₄F to N, P-TiO₂/S-TiN mass ratio is increased from 3 to the highest, 5 owing to the smallest TiN content to lose its electrical conductivity.

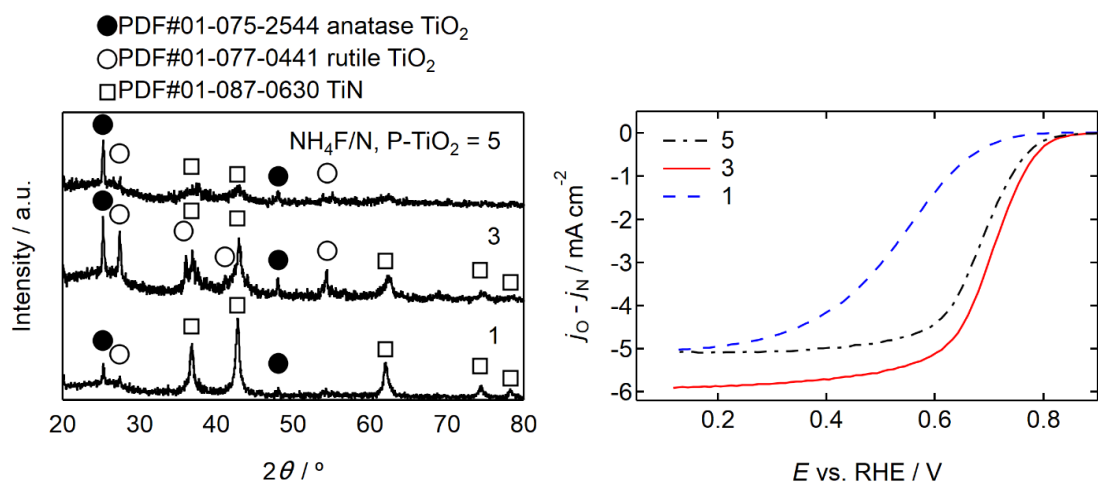


Fig. S6 (left) XRD patterns and (right) RDE voltammograms of N, P, S-TiO₂/S-TiN for three different mass ratios of NH₄F to N, P-TiO₂/S-TiN, at 1, 3 and 5. The NH₄F annealing was performed at 1,223 K for 1 h under N₂ with 0.5 dm³ min⁻¹. The scans were performed in N₂ and O₂, at a rotation speed of 1500 rpm and a cathodic scan rate of -5 mV s⁻¹ in 0.1 mol dm⁻³ H₂SO₄ solution.

S7. Effect of annealing conditions on the ORR activity of N, P, S-TiO₂/S-TiN catalysts

Fig. S7 shows RDE voltammograms of N, P, S-TiO₂/S-TiN synthesized at different temperatures, durations and N₂ gas flow rates during the annealing of NH₄F and N, P-TiO₂/S-TiN mixture at the optimized NH₄F to N, P-TiO₂/S-TiN mass ratio, 3 revealed in section S6. The optimized annealing conditions for the ORR activity of N, P, S-TiO₂/S-TiN are revealed to 1,223 K for 1 h under N₂ with 0.5 dm³ min⁻¹.

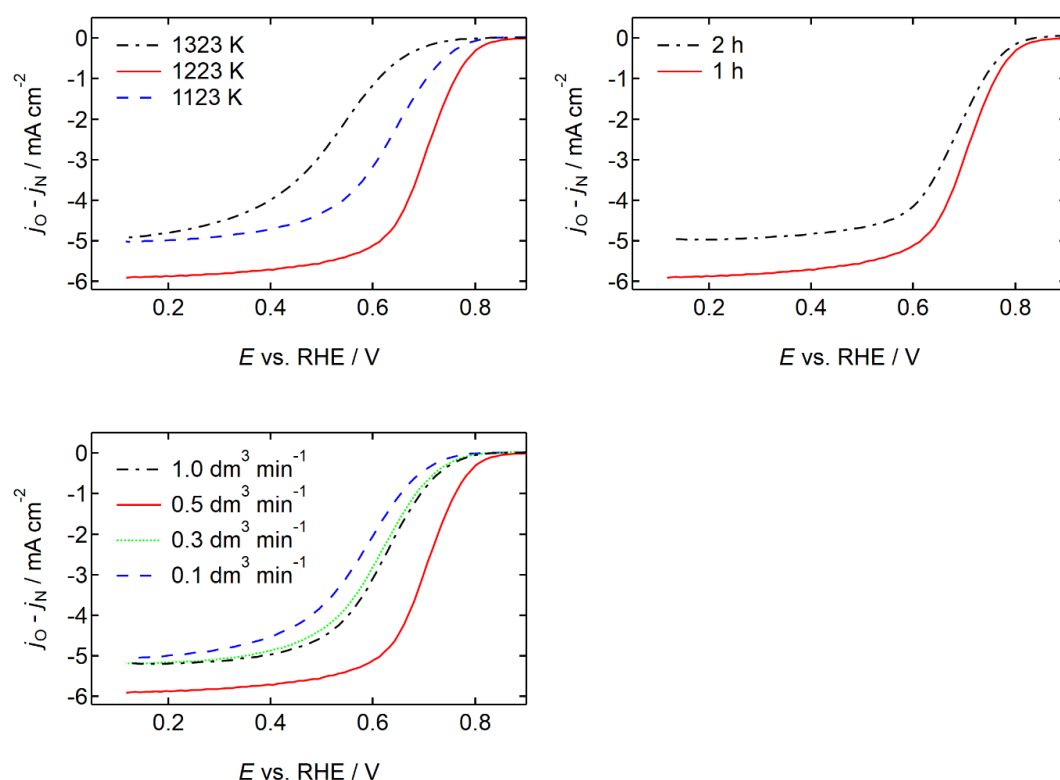


Fig. 7 RDE voltammograms of N, P, S-TiO₂/S-TiN for (left top) three different NH₄F-annealing temperatures at 1,123, 1,223 and 1,323 K for a fixed duration of 1 h under N₂ with 0.5 dm³ min⁻¹, (right top) two different NH₄F-annealing durations, 1 and 2 h at a fixed temperature of 1,223 K under N₂ with 0.5 dm³ min⁻¹ and (bottom) four different N₂ gas flow rates of 0.1, 0.3, 0.5 and 1.0 dm³ min⁻¹ during NH₄F-annealing at a fixed temperature and duration of 1,223 K and 1 h, respectively. The mass ratio of NH₄F to N, P-TiO₂/S-TiN was fixed at 3 for all the catalysts. The scans were performed in N₂ and O₂, at a rotation speed of 1,500 rpm and a cathodic scan rate of -5 mV s⁻¹ in 0.1 mol dm⁻³ H₂SO₄ solution.

S8. Effect of sulfur species on ORR activity of N, P, S-TiO₂/S-TiN

To reveal the role of sulfur species originated from the titanium source of N, P, S-TiO₂/S-TiN, TiOSO₄, it was replaced with a sulfur-free titanium source, (NH₄)₂TiF₆. Then N, P-TiO₂/TiN catalysts were synthesized under conditions identical to those of N, P, S-TiO₂/S-TiN catalysts which exhibited the highest ORR activity. Fig. S8 (left) shows XRD patterns of the N, P-TiO₂/TiN synthesized from (NH₄)₂TiF₆ before and after NH₄F-annealing at the optimized conditions revealed in section S6 and S7. A single TiN phase of N, P-TiO₂/TiN from (NH₄)₂TiF₆ before NH₄F-annealing is converted to a mixture of anatase/rutile TiO₂ and TiN phases after the NH₄F-annealing at 1,223 K under N₂ gas. The changes in crystal structure during NH₄F-annealing shown in Fig. S8 (left) are similar to those of N, P, S-TiO₂/S-TiN from TiOSO₄ shown in Fig. 1 (b). However, the activity is not similar as shown in Fig. S8 (right). The ORR activity of N, P, S-TiO₂/S-TiN from TiOSO₄ is much higher than N, P-TiO₂/TiN from (NH₄)₂TiF₆, indicating the necessity of sulfur species. The Tafel slope of N, P, S-TiO₂/S-TiN from TiOSO₄ and N, P-TiO₂/TiN from (NH₄)₂TiF₆ are 60 and 95 mV dec⁻¹, respectively. Although the RDE voltammograms were corrected with solution resistance measured by the Nyquist plots, the electrical resistance of catalyst layers could affect the voltammograms. The lower Tafel slope of N, P, S-TiO₂/S-TiN from TiOSO₄ would be due to the lower electrical resistance of the N, P, S-TiO₂/S-TiN when compared with N, P-TiO₂/TiN from (NH₄)₂TiF₆ as S-doping has been used to reduce the electrical resistance of TiO₂.^{S8, S9}

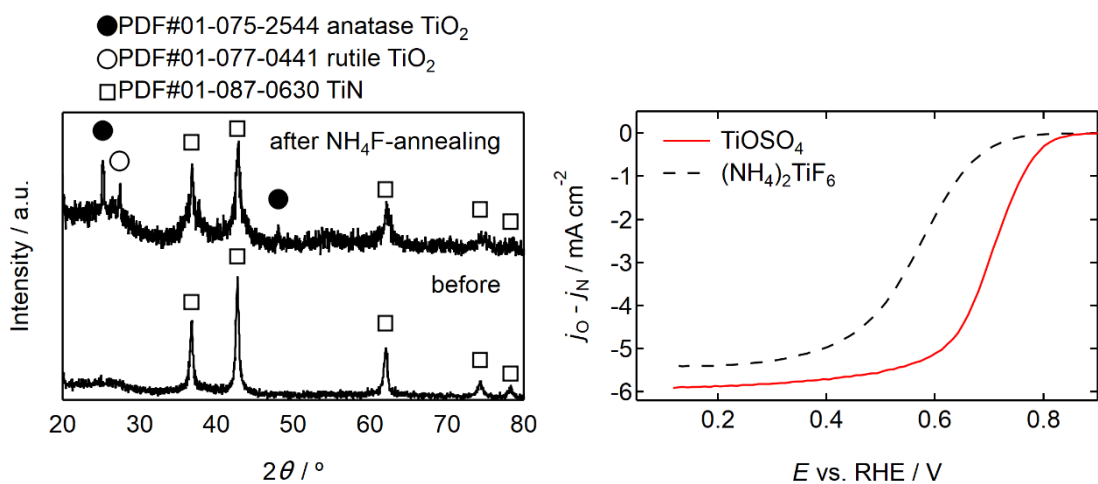


Fig. S8 (left) XRD patterns of N, P-TiO₂/S-TiN synthesized from (NH₄)₂TiF₆ before and after NH₄F-annealing and (right) RDE voltammograms of N, P-TiO₂/S-TiN and N, P, S-TiO₂/S-TiN synthesized from (NH₄)₂TiF₆ and TiOSO₄, respectively. For both two catalysts, the mass ratio of NH₄F to N, P-TiO₂/(S-)TiN was set at 3 and the NH₄F-annealing was performed at 1,223 K for 1 h under N₂ with 0.5 dm³ min⁻¹. The scans were performed in N₂ and O₂, at a rotation speed of 1500 rpm and a cathodic scan rate of -5 mV s⁻¹ in 0.1 mol dm⁻³ H₂SO₄ solution.

S9. Comparison of ORR activity of oxide, oxynitride and nitride catalysts in acidic media

The measure of ORR activity of non-PGM catalysts has not been standardized yet. A half-wave potential ($E_{1/2}$), i.e., the potential where half of the limiting current is obtained would be the fairest measure of activity and the values of oxide, oxynitride and nitride catalysts reported to date are compared in Table S1.

Table S1. ORR activity of carbon-supported/carbon-support-free oxide, oxynitride and nitride catalysts in acidic media.

Catalyst	Support	m^{*1}	ω^{*2}	ν^{*3}	Electrolyte	$E_{1/2}^{*4}$	source
N, P, S-TiO₂	S-TiN	0.86	1,500	5	0.1 mol dm⁻³ H₂SO₄	0.72	This work
N-ZrO ₂ (ZrO _x N _y)	Multi-walled carbon nanotube (MWCNT)	1.4	1,600	5	0.1 mol dm ⁻³ H ₂ SO ₄	0.70	S10
N, P-TiO ₂ (shell)	S-TiN (core)	0.86	1,500	5	0.1 mol dm ⁻³ H ₂ SO ₄	0.67	S3
TiO ₂	MWCNT	1.5	1,600	5	0.1 mol dm ⁻³ H ₂ SO ₄	0.64	S11
N-TiO ₂	Carbon black	1.0	1,500	5	0.1 mol dm ⁻³ H ₂ SO ₄	0.48	S12
N-TiO ₂	Ti ₄ O ₇	2.0	1,500	5	0.1 mol dm ⁻³ H ₂ SO ₄	0.63	S13
N-TiO ₂ (shell)	TiN (core)	2.0	1,500	5	0.1 mol dm ⁻³ H ₂ SO ₄	0.68	S14
N-TiO ₂ (shell)	Nitrided carbon (core)	0.28	1,600	10	0.5 mol dm ⁻³ H ₂ SO ₄	0.44	S15
Hf ₂ ON ₂	Carbon black	1.0	1,500	5	0.1 mol dm ⁻³ H ₂ SO ₄	0.54	S16
TaO _x	Carbon black	0.1	1,600	5	0.1 mol dm ⁻³ H ₂ SO ₄	0.60	S17
N-Ta ₂ O ₅	MWCNT	0.51- 0.57 ^{*5} (oxide)	1,600	5	0.1 mol dm ⁻³ H ₂ SO ₄	0.65	S18
Ta ₂ O ₅	MWCNT	1.6	1,600	5	0.1 mol dm ⁻³ H ₂ SO ₄	0.57	S19
N-Ta ₂ O ₅ /Ta ₃ N ₅ (shell)	Nitrided carbon (core)	0.28	1,600	10	0.5 mol dm ⁻³ H ₂ SO ₄	0.42	S20
Na ₂ Ta ₈ O _{21-x} / Ta ₂ O ₅ /Ta ₃ N ₅	Reduced graphene oxide	0.817	1,600	10	0.1 mol dm ⁻³ HClO ₄	0.42	S21
Co _{0.50} Mo _{0.50} O _y N _z (Co-Mo ₂ N)	Carbon black	0.7	1,600	10	0.1 mol dm ⁻³ HClO ₄	0.41	S22
CoWO _{1.2} N/CoN _x	Carbon black	0.142	2,000	5	0.5 mol dm ⁻³ H ₂ SO ₄	0.41	S23
Co _{0.50} Mo _{0.50} N _y	Nitrogen-doped carbon nanocage	0.097	2,500	10	0.5 mol dm ⁻³ H ₂ SO ₄	0.57	S24

*1 Catalyst (including support when used) loading in mg cm⁻².

*2 Rotation speed in rpm

*3 Scan rate in mV s⁻¹.

*4 Half-wave potential in V versus RHE.

*5 m , i.e., loading of N-Ta₂O₅ and MWCNT is not described and only N-Ta₂O₅ loading is available.

S10. Comparison of PGM-free catalysts' durability against startup/shutdown cycles of fuel cell vehicles (FCVs)

In most of the works on PGM-free catalysts, the durability against load cycles for FCVs, in which potential is cycled between 0.6 (load on) and 0.95/1.0 V (load off), have been evaluated. During the startup and shutdown of FCVs, the cathodes face with much more oxidative potentials up to 1.5 V by a so-called reverse-current decay mechanism as described in the main body of the text. For evaluating the durability against the startup and shutdown of FCVs, the Fuel Cell Commercialization Conference of Japan (FCCJ) first set the protocol, in which potential is cycled between 1.0 and 1.5 V at 0.5 V s^{-1} in an inert (N_2 - or Ar-saturated) acidic electrolyte.^{S2} The startup/shutdown durability test results of some limited number of PGM-free catalysts reported to date are compared in Table S2.

Table S2. Startup/shutdown durability of PGM-free catalysts in acidic media.

Catalyst	Electrolyte	Accelerated degradation test (ADT)				source
		Protocol	Cycle number	$\Delta E_{1/2}$ *	Limiting current plateau after ADT	
N, P, S-TiO₂/S-TiN	0.1 mol dm⁻³ H₂SO₄	1.0 V–1.5 V at 0.5 V s⁻¹	5,000	0.02 V	present	This work
N, P-TiO ₂ /S-TiN	0.1 mol dm ⁻³ H ₂ SO ₄	1.0 V–1.5 V at 0.5 V s ⁻¹	5,000	0.08 V	absent	S1
N-Ti _{0.8} Zr _{0.2} O ₂ /S-TiN	0.1 mol dm ⁻³ H ₂ SO ₄	1.0 V–1.5 V at 0.5 V s ⁻¹	5,000	0.04 V	absent	S25
Fe/N/C	0.1 mol dm ⁻³ HClO ₄	1.2 V–1.5 V at 0.5 V s ⁻¹	5,000	0.099 V	absent	S26
Fe/N/C	0.1 mol dm ⁻³ HClO ₄	1.0 V–1.5 V at 0.1 V s ⁻¹	6,200	0.27 V	absent	S27
Fe/N/C	0.5 mol dm ⁻³ H ₂ SO ₄	1.0 V–1.5 V at 0.5 V s ⁻¹	5,000	0.035 V	present	S28
Fe/N/C	0.5 mol dm ⁻³ H ₂ SO ₄	1.0 V–1.5 V at 0.5 V s ⁻¹	1,110	0.040 V	N/A	S29

* The $E_{1/2}$ difference between before and after the ADT cycles, $E_{1/2}$ (initial)– $E_{1/2}$ (after ADT cycles).

S11. Durability of other N, P, S-TiO₂/S-TiN catalysts against startup/shutdown cycles

Startup/shutdown durability of N, P, S-TiO₂/S-TiN catalysts synthesized under different NH₄F-annealing conditions was evaluated and the results are shown in Fig. S9. These catalysts display high durability against the startup/shutdown protocols in which E was cycled between 1.0 and 1.5 V and the difference in $E_{1/2}$ before and after 5,000 cycles is similar to that observed from Fig. 3, indicating the excellent repeatability in startup/shutdown durability. In Fig. S9 (left), the current density at $E \leq \sim 0.6$ V increased after the 5,000 cycles. Although the precise mechanism for the increase in current density is not clear at this stage, one of the reasons will be the removal of inactive species during the cycles to improve the mass transport properties, similar to the results reported by Wu *et al.*^{S30}

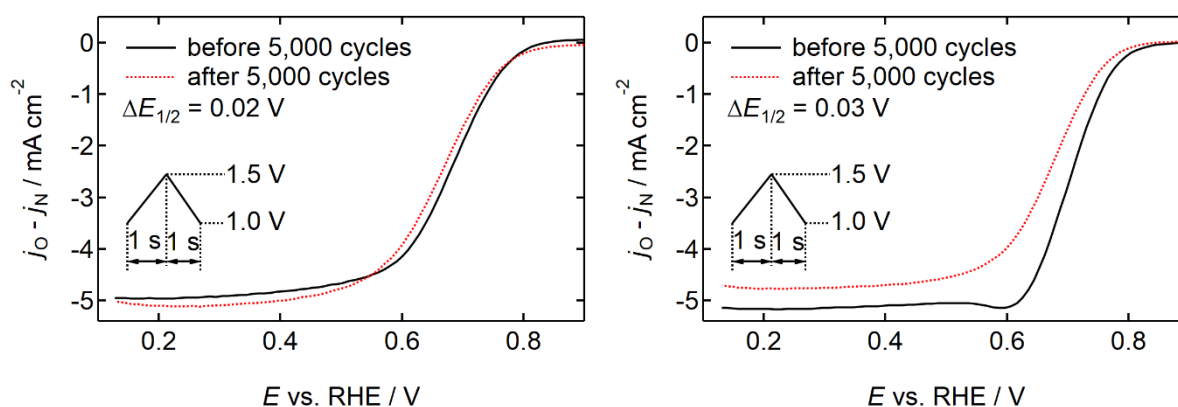


Fig. S9 RDE voltammograms of N, P, S-TiO₂/S-TiN catalysts before (solid curve) and after (dashed curve) 5,000 potential cycles between 1.0 and 1.5 V vs. reversible hydrogen electrode (RHE) at 0.5 V s⁻¹ in 0.1 mol dm⁻³ H₂SO₄ solution. Before and after 5,000 cycles, the scans were performed in N₂ and O₂ atmospheres at a rotation speed of 1,500 rpm and a cathodic scan rate of -5 mV s⁻¹ for evaluating the activity. The N, P, S-TiO₂/S-TiN catalysts were synthesized by annealing at 1,223 K for 2 h with the mass ratio of NH₄F to N, P-TiO₂/S-TiN of 3 (left) and at 1,223 K for 1 h with the mass ratio of NH₄F to N, P-TiO₂/S-TiN of 5 (right). In both cases, the annealing was performed under N₂ with 0.5 dm³ min⁻¹.

S12. Changes in crystal structure of N, P, S-TiO₂/S-TiN catalysts during ORR

Stability of N, P, S-TiO₂/S-TiN catalyst's crystal structure was evaluated by XRD patterns shown in Fig. S10. Catalyst layers after electrochemical ORR tests were carefully peeled off from the GC disk electrodes. The XRD pattern shown in the top of Fig. S10 is from N, P, S-TiO₂/S-TiN particles and Nafion used in the catalyst layers. All the peaks observed from as prepared N, P, S-TiO₂/S-TiN without Nafion shown in the bottom of Fig. S10 retained during ORR tests, indicating that the all the phases are stable.

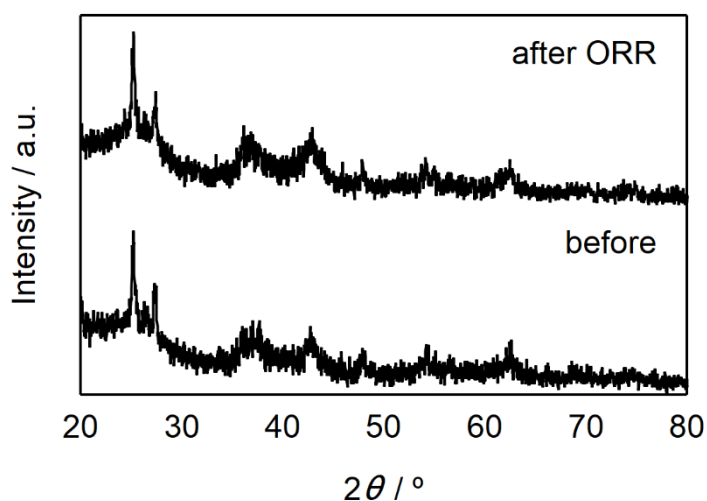


Fig. S10 XRD patterns of N, P, S-TiO₂/S-TiN catalyst (bottom) before and (top) after ORR tests.

S13. Changes in morphology of N, P, S-TiO₂/S-TiN catalysts during startup/shutdown cycles

Fig. S11 shows TEM images of N, P, S-TiO₂/S-TiN catalysts before and after 5,000 startup/shutdown cycles. Thin sheets remained during the cycles, indicating the morphological stability of N, P, S-TiO₂/S-TiN. Because N, P, S-TiO₂/S-TiN catalysts after 5,000 cycles contains Nafion ionomer, clear high resolution images could not be obtained.

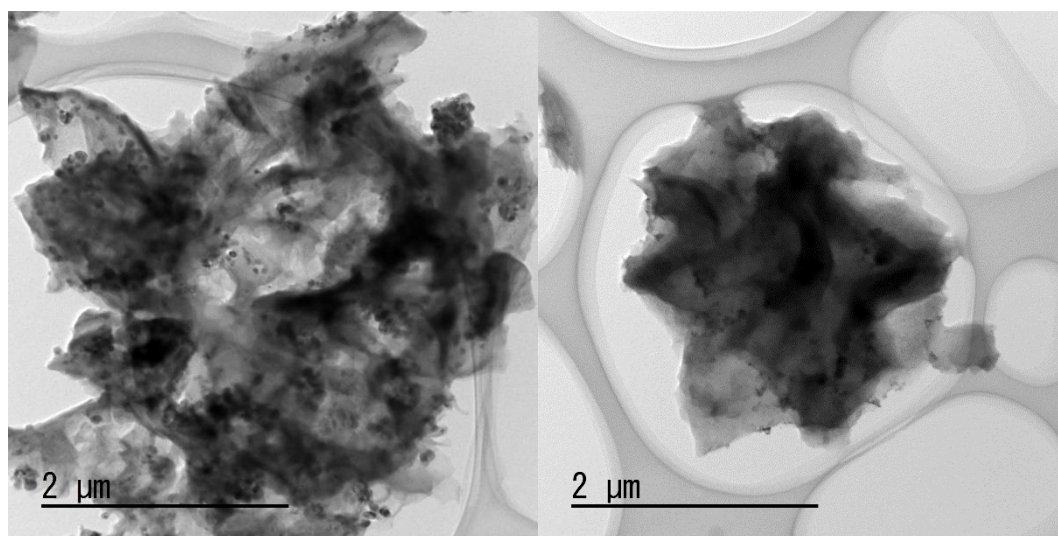


Fig. S11 TEM images of N, P, S-TiO₂/S-TiN catalysts before (left) and after (right) 5,000 potential cycles between 1.0 and 1.5 V vs. reversible hydrogen electrode (RHE) at 0.5 V s⁻¹ in 0.1 mol dm⁻³ H₂SO₄ solution. The N, P, S-TiO₂/S-TiN catalyst after 5,000 cycles contains Nafion ionomer used in the catalyst layer.

Supporting References

- S1 M. Chisaka, R. Xiang, S. Maruyama and H. Daiguji, *ACS Appl. Energy Mater.*, 2020, **3**, 9866.
- S2 A. Ohma, K. Shinohara, A. Iiyama, T. Yoshida and A. Daimaru, *ECS Trans.*, 2011, **41**, 775.
- S3 M. Chisaka and H. Morioka, *Catal. Sci. Technol.*, 2019, **9**, 611.
- S4 M. Chisaka, Y. Suzuki, T. Iijima, Y. Ishihara, R. Inada and Y. Sakurai, *ECS Electrochem. Lett.*, 2012, **3**, F1.
- S5 D. A. H. Hanaor and C. C. Sorrell, *J. Mater. Sci.*, 2011, **46**, 855.
- S6 J. C. Yu, J. Yu, W. Ho, Z. Jiang and L. Zhang, *Chem. Mater.*, 2002, **14**, 3808.
- S7 F. Cardarelli, in *Materials Handbook: A Concise Desktop Reference*, 2nd ed., (Ed. F. Cardarelli), Springer-Verlag, London, UK, 2008, Ch. 10.
- S8 J. Ni, S. Fu, C. Wu, J. Maier, Y. Yu and L. Li, *Adv. Mater.*, 2016, **28**, 2259.
- S9 W. Jiao, N. Li, L. Wang, F. Li, G. Liu and H. M. Cheng, *Chem. Commun.*, 2013, **49**, 3461.
- S10 M. Chisaka, A. Ishihara, H. Morioka, T. Nagai, S. Yin, Y. Ohgi, K. Matsuzawa, S. Mitsushima and K. Ota, *ACS Omega*, 2017, **2**, 678.
- S11 T. Hayashi, A. Ishihara, N. Uehara, Y. Kohno, K. Matsuzawa, S. Mitsushima and K. Ota, *Electrochemistry*, 2015, **83**, 807.
- S12 M. Chisaka, Y. Ando and N. Itagaki, *J. Mater. Chem. A*, 2016, **4**, 2501.
- S13 M. Chisaka, Y. Ando, Y. Yamamoto and N. Itagaki, *Electrochim. Acta*, 2016, **214**, 165.
- S14 M. Chisaka, Y. Yamamoto, N. Itagaki and Y. Hattori, *ACS Appl. Energy Mater.*, 2018,

1, 211.

S15 M. Wassner, M. Eckardt, C. Gebauer, N. Hüsing and J. Behm, *ChemElectroChem*, 2016, **3**, 1641.

S16 M. Chisaka, Y. Suzuki, T. Iijima and Y. Sakurai, *J. Phys. Chem. C*, 2011, **115**, 20610.

S17 J. Seo, D. H. Anjum, K. Takanabe, J. Kubota and K. Domen, *Electrochim. Acta*, 2014, **149**, 76.

S18 N. Uehara, A. Ishihara, T. Nagai, M. Matsumoto, H. Imai, Y. Kohno, K. Matsuzawa, S. Mitsushima and K. Ota, *Electrochim. Acta*, 2015, **182**, 789.

S19 A. Ishihara, M. Chisaka, Y. Ohgi, K. Matsuzawa, S. Mitsushima and K. Ota, *Phys. Chem. Chem. Phys.*, 2015, **17**, 7643.

S20 M. Wassner, M. Eckardt, C. Gebauer, G. R. Bourret, N. Hüsing and R. J. Behm, *Electrochim. Acta*, 2017, **227**, 367.

S21 G. Zhang, D. Sebastián, X. Zhang, Q. Wei, C. Lo Vecchio, J. Zhang, V. Baglio, W. Wang, S. Sun, A. S. Aricò and A. C. Tavares, *Adv. Energy Mater.*, 2020, **10**, 2000075.

S22 B. Cao, G. M. Veith, R. E. Diaz, J. Liu, E. A. Stach, R. R. Adzic and P. G. Khalifah, *Angew. Chem. Int. Ed. Engl.*, 2013, **52**, 10753.

S23 T. Ando, S. Izhar, H. Tominaga and M. Nagai, *Electrochim. Acta*, 2010, **55**, 2614.

S24 T. Sun, Q. Wu, R. Che, Y. Bu, Y. Jiang, Y. Li, L. Yang, X. Wang and Z. Hu, *ACS Catal.*, 2015, **5**, 1857.

S25 M. Chisaka, R. Xiang, S. Maruyama and H. Daiguji, *Energy Fuels*, 2022, **36**, 539.

S26 C. H. Choi, C. Baldizzone, J. P. Grote, A. K. Schuppert, F. Jaouen and K. J. J. Mayrhofer, *Angew. Chem. Int. Ed. Engl.*, 2015, **54**, 12753.

S27 K. Strickland, E. Miner, Q. Jia, U. Tylus, N. Ramaswamy, W. Liang, M. T. Sougrati, F. Jaouen and S. Mukerjee, *Nat. Commun.*, 2015, **6**, 7343.

S28 X. Zhao, X. Yang, M. Wang, S. Hwang, S. Karakalos, M. Chen, Z. Qiao, L. Wang, B. Liu, Q. Ma, D. A. Cullen, D. Su, H. Yang, H. Y. Zang, Z. Feng and G. Wu, *Appl. Catal. B*,

2020, **279**, 119400.

S29 A. Muthukrishnan, Y. Nabaе, T. Hayakawa, T. Okajima, T. Ohsaka, *Catal. Sci. Technol.*, 2015, **5**, 475.

S30 G. Wu, K. L. More, C. M. Johnston and P. Zelenay, *Science*, 2011, **332**, 443.